PCCP

Cite this: *Phys. Chem. Chem. Phys.*, 2011, **13**, 4411–4419

www.rsc.org/pccp

**PAPER**



# $Eu^{3+}$-doped β-$Ga_2O_3$ nanophosphors: annealing effect, electronic structure and optical spectroscopy†

**Haomiao Zhu,[ab] Renfu Li,[ab] Wenqin Luo[ab] and Xueyuan Chen*[ab]**

***Received 13th November 2010, Accepted 17th December 2010***
**DOI: 10.1039/c0cp02520h**

A comprehensive survey of electronic structure and optical properties of rare-earth ions-doped semiconductor is of vital importance for their potential applications. In this work, $Eu^{3+}$-doped β-$Ga_2O_3$ nanocrystals were synthesized *via* a combustion method. The evolution of the optical properties of nanophosphors with increasing the annealing temperature was investigated in detail by means of excitation and emission spectra at room temperature and 10 K. $Eu^{3+}$ ions were proved to be incorporated into the crystal lattice of the β-$Ga_2O_3$ phase after annealing the as-prepared nanoparticles at 1100 °C. It was observed that the substitution of $Eu^{3+}$ for $Ga^{3+}$ occurred at merely single site, in spite of two crystallographically nonequivalent sites of $Ga^{3+}$ in β-$Ga_2O_3$. Spectroscopic evidence corroborated and clarified the local symmetry of $C_s$ for $Eu^{3+}$ at this single site. From the high-resolution excitation and emission spectra, 71 crystal-field levels of $Eu^{3+}$ in β-$Ga_2O_3$ were identified and analyzed in terms of 19 freely varied free-ions and crystal-field parameters based on $C_s$ symmetry. The standard deviation of the final fitting is as low as 12.9 $cm^{-1}$, indicating an excellent agreement between experimental and calculated energy levels. The temperature-dependent luminescence dynamics of the $^5D_0$ multiplet for $Eu^{3+}$ in β-$Ga_2O_3$ phosphors has also been revealed for the first time from 10 to 300 K.

## 1. Introduction

Rare-earth (RE)-doped semiconductor nanocrystals (NCs) have attracted considerable attention in the past decade for their ability to tailor the optical properties *via* size control and to achieve efficient RE luminescence sensitized by exciton recombination in the host. These unique optical properties enable them to have potential applications in areas as diverse as full color display,[1,2] biolabels,[3] and phosphors.[4–7] Gallium oxide ($Ga_2O_3$) has five crystal structures and β-$Ga_2O_3$ is the most stable phase, which is a semiconductor with a wide band gap of ~4.8 eV.[8,9] The structure of β-$Ga_2O_3$ is monoclinic with a space group of $C2/m$, and $Ga^{3+}$ ions occupy two crystallographic sites, namely tetrahedral and octahedral, respectively.[10] β-$Ga_2O_3$ has been reported as a promising material for applications in the fields such as high temperature gas sensor,[11,12] catalyst,[13] and optoelectronic devices.[14] Great efforts have been made to investigate the optical properties of $Ga_2O_3$, including the origin of the self-activated luminescence,[15–18] the emission of the impurity nitrogen[19,20] and the optical properties of various nanostructured materials such as nanowires[21] and nanobelts.[22]

Recently it has been realized that β-$Ga_2O_3$ is also a good host for RE ions due to their high thermal and chemical stability and a wide range of optical transparency. The wide band gap of the host may allow us to improve the luminescence efficiency of RE emissions.[23] The large refraction index of β-$Ga_2O_3$ (1.85–1.91) combined with the RE luminescence makes RE-doped β-$Ga_2O_3$ attractive for waveguiding applications.[24] Up to now, the visible and infrared luminescence of $Er^{3+}$ in β-$Ga_2O_3$ have been occasionally reported with either photon or electron excitation.[14,24–27] $Dy^{3+}$-doped β-$Ga_2O_3$ synthesized with various morphologies showed a morphology-dependent optical properties,[28] and efficient host-to-$Dy^{3+}$ energy transfer (ET).[28,29] The codoping of $Li^+$ was proved to be able to enhance the photoluminescence (PL) intensity of $Dy^{3+}$ in β-$Ga_2O_3$.[30] It is expected that, by integrating the distinct optical properties of $Eu^{3+}$, $Eu^{3+}$-doped β-$Ga_2O_3$ is of particular interest for bioprobes, lighting and displays applications. The electroluminescence devices based on $Eu^{3+}$-doped $Ga_2O_3$ thin films were demonstrated with relatively low threshold voltage.[31–34] $Eu^{3+}$-doped $Ga_2O_3$ NCs and phosphors were also synthesized by a variety of

[a] *Key Laboratory of Optoelectronic Materials Chemistry and Physics, Fujian Institute of Research on the Structure of Matter, Chinese Academy of Sciences, Fuzhou, Fujian 350002, China. E-mail: xchen@fjirsm.ac.cn; Fax: +86 591-8764-2575; Tel: +86 591-8764-2575*
[b] *State Key Laboratory of Structural Chemistry, Fuzhou, Fujian 350002, China*

† Electronic supplementary information (ESI) available: TEM and SAED images of the sample annealed at 650 °C; RT emission spectrum of 0.1 at% $Eu^{3+}$ doped β-$Ga_2O_3$ annealed at 650 °C upon excitation at 285 nm; RT emission spectra of the sample annealed at 1000 °C before and after washing with diluted $HNO_3$ upon excitation at 285 nm. See DOI: 10.1039/c0cp02520h

methods and their PL properties have been characterized preliminarily.[35–39] However, the $Eu^{3+}$ emission and excitation spectra presented in those works showed a broadband behavior rather than sharp transition lines that were typical of $Eu^{3+}$ in a crystalline environment, indicating that $Eu^{3+}$ ions might be located at the surface or close to the surface sites instead of entering the crystal lattice of β-$Ga_2O_3$. To date, the electronic structure and detailed optical properties, such as luminescence dynamics and site symmetry analysis of $Eu^{3+}$ ions in the β-$Ga_2O_3$ lattice, are still lacking. Therefore, further systematical investigation of the optical properties of $Eu^{3+}$ in β-$Ga_2O_3$ is of vital importance for their future applications.

In this work, we will present the synthesis of $Eu^{3+}$-doped β-$Ga_2O_3$ NCs *via* a simple combustion method. The correlation between the optical properties and annealing conditions, local site symmetry and PL dynamics of $Eu^{3+}$ in β-$Ga_2O_3$ NCs will be investigated in detail. Spectroscopic evidence will be provided for the incorporation of $Eu^{3+}$ into the β-$Ga_2O_3$ lattice, and crystal-field (CF) analysis for the observed energy levels in this new kind of phosphors will be carried out for the first time.

## 2. Experimental details

### 2.1 Nanocrystal synthesis

$Eu^{3+}$-doped β-$Ga_2O_3$ NCs were synthesized by a combustion method reported by Mahalingam *et al.*[40] The $Ga_2O_3$ (AR), $Eu(NO_3)_3{\cdot}6H_2O$ (AR) and glycine (AR) were used as raw chemicals. The synthesis procedure for 1 at% $Eu^{3+}$-doped β-$Ga_2O_3$ samples was briefed as follows. Firstly, 0.3711 g $Ga_2O_3$ was dissolved in diluted nitric acid and the solution was evaporated at 70 °C until $Ga(NO_3)_3{\cdot}xH_2O$ was obtained. Then 0.0178 g $Eu(NO_3)_3{\cdot}6H_2O$, 0.3603 g glycine and 25 mL distilled water were added. The resultant solution was stirred for 10 h and then evaporated at 120 °C in an oven. When a transparent residue was formed the temperature was increased to 220 °C and the combustion reaction took place. The as-prepared products were then annealed under various conditions in air, that is, 650 °C for 5 h, 900 °C for 5 h, 1000 °C for 10 h and 1100 °C for 24 h, respectively.

### 2.2 Characterization

The phase identification of the samples was performed by powder X-ray diffraction (XRD) using a Miniflex II diffractometer with Cu Kα1 radiation ($\lambda$ = 0.154 nm). The morphologies of the NCs were characterized by a JEOL-2010 transmission electron microscopy (TEM). The excitation and emission spectra and transient decays were measured using an Edinburgh Instrument FLS920 spectrometer equipped with both continuous (450 W) and microsecond pulsed xenon (Xe) lamps. For low temperature (10 K) experiments, the sample was mounted on an optical cryostat (10–350 K, DE202, Advanced Research Systems). For laser excited PL measurements, a frequency doubling Ti:sapphire laser (700–1000 nm, pulse width $\leq$ 1.5 ps, Tsunami, Spectra Physics) was used for excitation. All the spectra were corrected for the instrument response.

## 3. Results and discussion

### 3.1 Structural and morphology characterization

The XRD pattern of the 1 at% $Eu^{3+}$-doped sample annealed at 650 °C was shown in Fig. 1. It can be seen that the pattern is in line with the *C*2/*m* space group of β-$Ga_2O_3$ (JCPDS NO. 43-1012). This is consistent with the result that the β phase can be formed under the annealing temperature higher than 600 °C.[29,41] However, the barely resolved diffraction peaks indicate very small size of NCs. TEM images of this sample show that the NCs are aggregated but clear crystalline lattice fringes can be observed. The selected-area electron diffraction (SAED) pattern exhibits a polycrystalline nature and the diffraction rings can be well indexed to the (002), (111), ($\bar{1}$12) and (710) planes of β-$Ga_2O_3$ (Fig. S1 in the ESI†). The clear crystalline lattice fringes and diffraction rings suggest that the samples annealed at 650 °C were well crystallized. The XRD patterns of 1 at% $Eu^{3+}$-doped samples annealed at higher temperatures are also shown in Fig. 1 for comparison. Obviously, the NCs grow larger with higher annealing temperature and longer annealing time. The average diameters estimated by Debye–Scherrer's formula are 5, 20, 30 and 45 nm for samples annealed at 650, 900, 1000 and 1100 °C , respectively.

### 3.2 Excitation and emission spectra

Fig. 2 shows the room temperature (RT) excitation and emission spectra of the 1 at% $Eu^{3+}$-doped sample annealed at 650 °C. When excited at 285 nm, as shown in Fig. 2(a), all the emissions were originated from the $^5D_0$ multiplet of $Eu^{3+}$. No emissions from the $^5D_1$ and $^5D_2$ multiplets were observed, even in 0.1 at% $Eu^{3+}$-doped counterparts (Fig. S2 in the ESI†), in which the concentration quenching can be neglected. This suggests an efficient multiphonon relaxation from the upper exited states to $^5D_0$. When monitored the $^5D_0 \rightarrow {}^7F_2$ emission, the excitation spectrum in a range of 230–550 nm was shown in Fig. 2(b). In addition to the sharp 4f-shell inner transitions from $^7F_0$ to $^5D_{1,2,3,4}$ and $^5L_6$ of $Eu^{3+}$, a strong and broad excitation band centered at 285 nm with a full width at

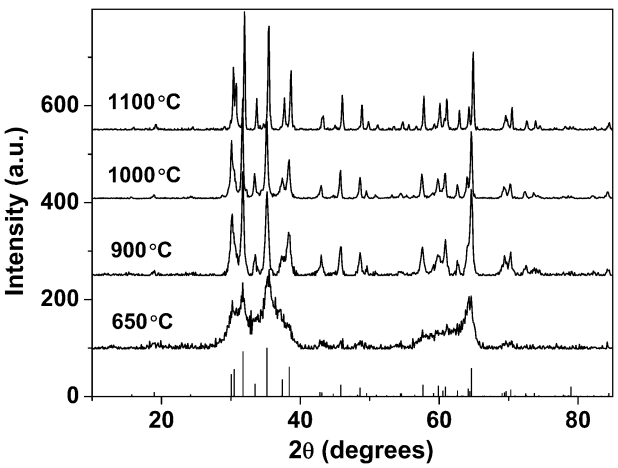


**Fig. 1** XRD patterns of 1 at% $Eu^{3+}$-doped β-$Ga_2O_3$ annealed at various conditions. The bars represent the standard XRD data of β-$Ga_2O_3$ (JCPDS NO. 43-1012).

 

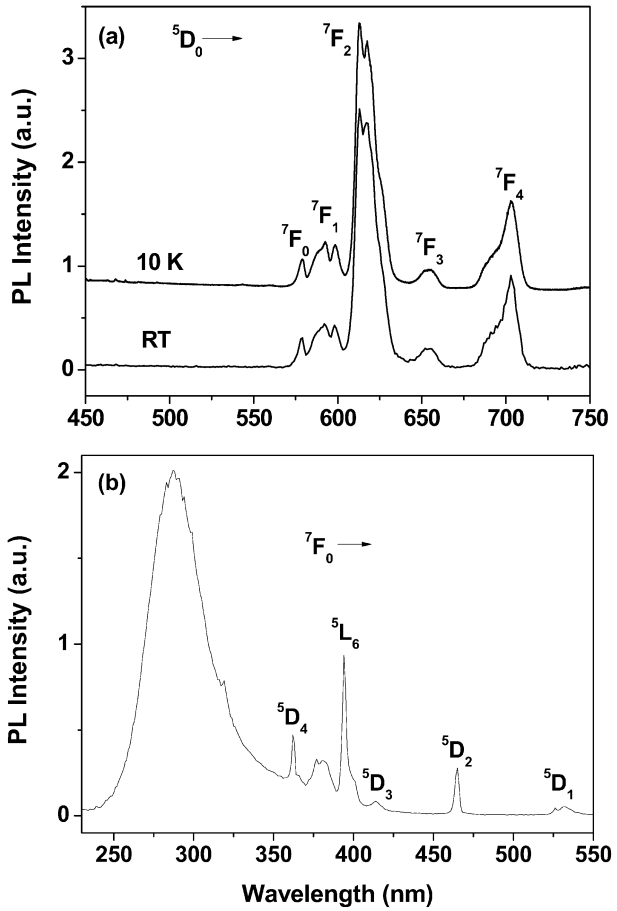


**Fig. 2** (a) Emission spectra at RT and 10 K, and (b) excitation spectrum at RT for the 1 at% $Eu^{3+}$-doped sample annealed at 650 °C. The $^5D_0 \rightarrow {}^7F_2$ emission was monitored in the excitation spectrum. The emission spectrum was measured upon excitation at 285 nm.

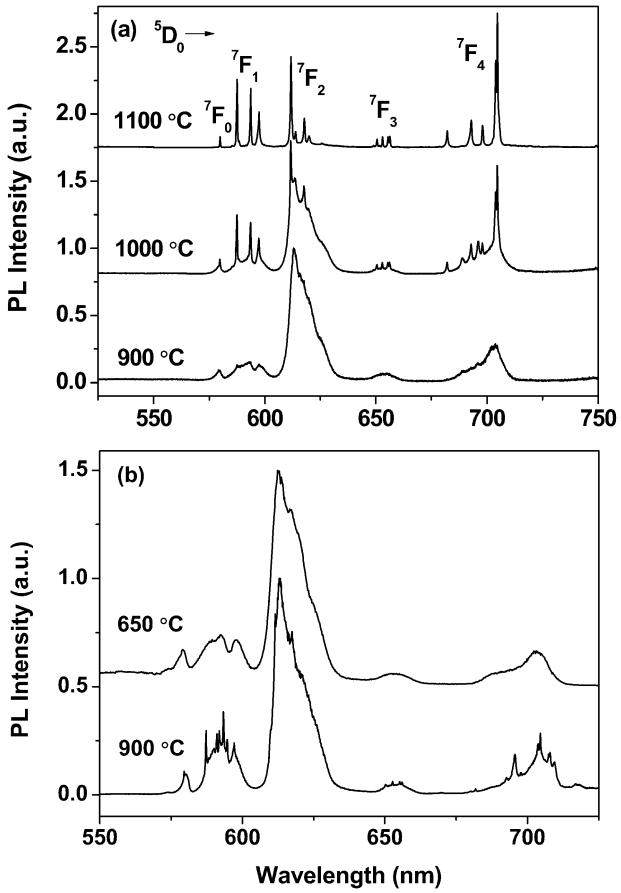


**Fig. 3** (a) The 10 K emission spectra upon excitation at ~270 nm with a Xe lamp for the samples annealed at 900, 1000 and 1100 °C, respectively. (b) The 10 K emission spectra upon laser excitation at 394 nm for the samples annealed at 650 and 900 °C, respectively.

half maximum (FWHM) of 40 nm was observed. It was reported that in $Dy^{3+}$-doped β-$Ga_2O_3$ NCs the $Dy^{3+}$ luminescence can be sensitized by the host with a broad excitation band centered at 257 nm, corresponding to the ~4.8 eV band gap of β-$Ga_2O_3$.[29] However, in this case, the energy of the excitation peak is lower than the band gap of β-$Ga_2O_3$. The possible reasons for the red shift of this excitation band will be discussed later. Fig. 2(a) also shows the 10 K emission spectra of the sample annealed at 650 °C for comparison. As we can see, no resolved emission lines between the CF levels of $Eu^{3+}$ can be observed at 10 K. The emission spectra at 10 K and RT remain essentially unchanged. This phenomenon means that the spectra were broadened inhomogeneously, in other words, these emissions may arise mainly from the $Eu^{3+}$ ions that occupied a surface or near surface site.

To investigate the annealing effect on the optical properties of $Eu^{3+}$ in β-$Ga_2O_3$, the 10 K emission spectra of 1 at% $Eu^{3+}$-doped samples annealed at 900, 1000, and 1100 °C were measured and shown in Fig. 3(a), respectively. It shows clearly that, different from the sample annealed at 900 °C, the other two counterparts exhibit sharp and well-resolved transition lines, revealing that more $Eu^{3+}$ ions were incorporated into the crystal lattices as the annealing temperature increased gradually. The absence of sharp lines for the sample annealed at 900 °C is probably due to the fact that only a small portion of $Eu^{3+}$ ions was in the NC lattices and the related emission is too weak to be observed under Xe lamp excitation. To prove this, the emission spectra of the samples annealed at 650 and 900 °C were measured at 10 K using a frequency doubling Ti:sapphire laser at 394 nm as the pump source. As shown in Fig. 3(b), no sharp transition lines were observed for the sample annealed at 650 °C even under laser excitation, suggesting that much less $Eu^{3+}$ ions in this sample entered into the crystal lattice. By contrast, sharp transition lines of $Eu^{3+}$ emerged for the sample annealed at 900 °C, verifying that a small portion of $Eu^{3+}$ ions was indeed incorporated into the crystal lattice. For NCs, the ratio of surface-to-volume increases with decreasing particle size. Consequently more $Eu^{3+}$ ions are located close to the surface in smaller NCs. Due to more serious structural defects near the surface, those $Eu^{3+}$ ions may experience various CF environments and their PL spectra will be broadened inhomogeneously. With the NC growth, the portion of the $Eu^{3+}$ ions on the surface or near the surface decreases that gives rise to much sharper PL emission lines. It is worthy of noting that only broad and unresolved emission bands analogous to that of the sample annealed at 650 °C (Fig. 2) were observed at RT for $Eu^{3+}$-doped β-$Ga_2O_3$

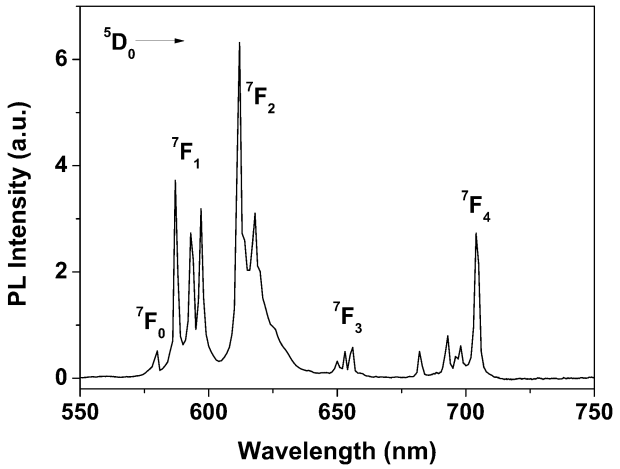


**Fig. 4** RT emission spectrum upon excitation at 266 nm for the sample annealed at 1100 °C.

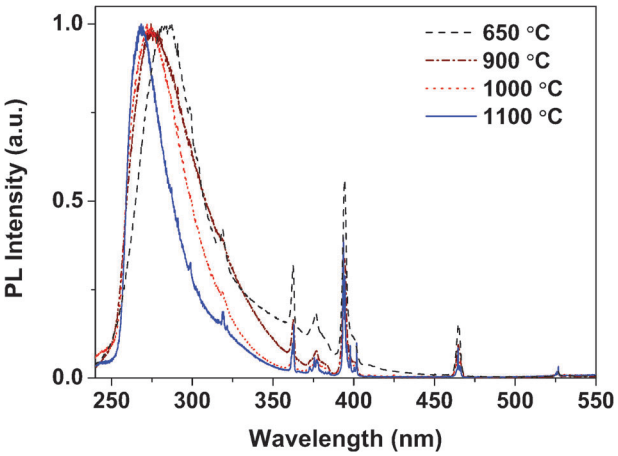


**Fig. 5** The 10 K excitation spectra by monitoring $^5D_0 \rightarrow {}^7F_2$ emission of $Eu^{3+}$ for the samples annealed at 650, 900, 1000 and 1100 °C, respectively.

previously reported.[31,33,35–39,42] In sharp contrast, much sharper transition lines of $Eu^{3+}$ (with a FWHM of ~1.5 nm) can be observed at RT for the sample annealed at 1100 °C (Fig. 4). This further confirms the successful incorporation of $Eu^{3+}$ ions into the β-$Ga_2O_3$ lattice. Note that the RT and 10 K emission lines of the sample annealed at 1100 °C are markedly different from those of the $Eu_2O_3$ polycrystalline powders in terms of peak positions and shapes,[43,44] therefore the formation of the $Eu_2O_3$ clusters or impurities in the sample can be ruled out. To verify the above assumption that the broad emissions arise mainly from $Eu^{3+}$ ions close to the surface. The samples annealed at 650 and 1000 °C were intentionally washed with diluted $HNO_3$ to investigate the surface effects on their PL spectra. After washing with $HNO_3$, the emission spectrum of the sample annealed at 1000 °C was indeed improved, sharper than that measured before washing (Fig. S3 in the ESI†). For the sample annealed at 650 °C, the emission spectrum remains essentially unchanged before and after washing. This is also reasonable since few $Eu^{3+}$ ions were in the lattice of β-$Ga_2O_3$, therefore washing the NCs with $HNO_3$ does not change the spectrum.

Fig. 5 compares the 10 K excitation spectra of the samples annealed at 650, 900, 1000 and 1100 °C by monitoring the $^5D_0 \rightarrow {}^7F_2$ emission. With increasing the annealing temperature, the peak of the broad excitation band is blue shifted from 285 to 266 nm, which is close to the ~4.8 eV band gap of β-$Ga_2O_3$. Simultaneously, the FWHM of the band decreases with higher annealing temperature. Previously, similar broad excitation bands peaked at very different wavelengths were observed in $Eu^{3+}$-doped β-$Ga_2O_3$, for example, ~305 nm for the nanophosphors synthesized by a sol–gel method,[38,39] ~280 nm for bulk crystals synthesized by a solid state reaction method,[38] ~270 nm for thin films prepared by chemical bath deposition,[42] and ~257 nm for thin films prepared by pulsed laser deposition.[34] For laser deposited films, the excitation band at ~257 nm was ascribed to the band gap transition of the host, while those of other samples were assigned to the $Eu^{3+}$–$O^{2-}$ charge transfer transition. For $Dy^{3+}$ and $Er^{3+}$-doped β-$Ga_2O_3$, the broad excitation bands with peaks at ~255 nm were also observed when monitoring the RE emission and considered as the band gap transition of the host.[25,28,29] The polarized absorption or excitation spectra of β-$Ga_2O_3$ single crystals were measured and the absorption band edges were found to be dependent on the electric field orientation ($E$) of the excitation light due to the anisotropy of the monoclinic structure. Binet and Gourier[16] reported the absorption edges located at 4.7 and 4.6 eV for $E//b$ and $E \perp b$ ($b$ represents the two fold crystallographic axis of β-$Ga_2O_3$), respectively. Ueda *et al.*[9] evidenced that the absorption band edges were 4.9 and 4.7 eV for $E//b$ and $E \perp b$, respectively. Moreover, the band gap widening was observed with the increase of the carrier concentration.[45] Therefore, the band gap of β-$Ga_2O_3$ may differ under different synthesis conditions such as the growth atmosphere, annealing time and impurity doping. The excitation band at 266 nm that we observed is falling in the range of the reported band gap values and thus can be attributed to the band gap transition of the host.[8,9,16,46] The blue shifting of the excitation peak is very likely owing to the decrease of the defect concentration in β-$Ga_2O_3$ annealed at higher temperatures, since the defect (oxygen or gallium vacancies) excitation bands with energies slightly below the band gap were observed in β-$Ga_2O_3$.[16,46] As shown in Fig. 5, the excitation band at 266 nm is much stronger than that of the 4f–4f transitions of $Eu^{3+}$, suggesting an efficient host-to-$Eu^{3+}$ ET.

### 3.3 Local site symmetry of $Eu^{3+}$

The following site symmetry analysis is based on the sample annealed at 1100 °C, in which most $Eu^{3+}$ ions were proved to reside in the crystal lattice as discussed above. It is well-known that the $^5D_0 \rightarrow {}^7F_2$ transition of the $Eu^{3+}$ ions is of electric-dipole (ED) nature and hypersensitive to the site symmetry but the $^5D_0 \rightarrow {}^7F_1$ transition is of magnetic-dipole (MD) and insensitive to the site symmetry. According to the selection rules of the ED transition, the $^5D_0 \rightarrow {}^7F_2$ transition is allowed only when the $Eu^{3+}$ ions occupy a site without an inversion center. As shown in Fig. 3(a), the ratio of the integrated PL intensities of the $^5D_0 \rightarrow {}^7F_2$ and $^5D_0 \rightarrow {}^7F_1$ transitions is 1.4 for the sample annealed at 1100 °C. Therefore, the $Eu^{3+}$

 

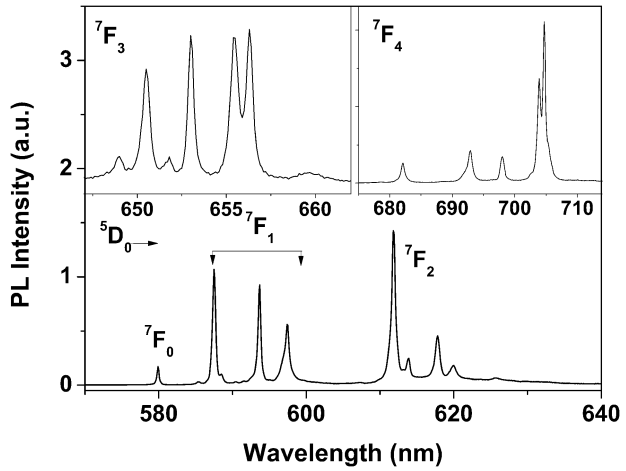


**Fig. 6** High-resolution emission spectra at 10 K upon band gap excitation for the sample annealed at 1100 °C.

ions most probably occupy a site without an inversion center. Moreover, on the basis of the selection rules of ED and MD transitions, the allowed $^5D_0 \rightarrow {}^7F_J$ ($J$ = 0, 1, 2, 3, 4, 5, and 6) transition lines in 32 crystallographic point groups can be obtained.[47] By comparing the observed transition lines with the theoretical numbers, we can assign the possible $Eu^{3+}$ site symmetries from the measured 10 K emission spectrum. Fig. 6 shows the enlarged 10 K emission spectra of the sample annealed at 1100 °C. The emission spectra were collected upon excitation above the band gap of β-$Ga_2O_3$, therefore all the $Eu^{3+}$ ions will be excited through host-to-$Eu^{3+}$ ET provided that $Eu^{3+}$ ions occupy multiple sites in the crystal lattices. The numbers of the observed transition lines of the $^5D_0 \rightarrow {}^7F_0$, $^7F_1$, $^7F_2$, $^7F_3$ and $^7F_4$ transitions are 1, 3, 5, 7 and 5, respectively. We further measured the luminescence decay curves at 10 K by monitoring the four emission lines of the $^5D_0 \rightarrow {}^7F_0$, $^7F_1$ transitions, respectively. The decay curves are exactly the same, verifying that these emissions were originated from the same $Eu^{3+}$ resided in a single lattice site. Based on the above spectroscopic evidence, the highest local site symmetry of $Eu^{3+}$ is deduced to be $C_s$ or $C_2$.

It should be noted that the $Ga^{3+}$ ions occupy two crystallographic sites in β-$Ga_2O_3$, tetrahedral (coordinated with four oxygen ions) and octahedral (coordinated with six oxygen ions). In several papers concerning the local site symmetry of RE ions in β-$Ga_2O_3$, these two sites were assigned with $T_d$ (tetrahedral site) and $O_h$ (octahedral site) symmetries, respectively.[29,30,36,37] However, according to the crystal structure of β-$Ga_2O_3$,[10] the tetrahedron and octahedron are not regular but distorted and the real point-group of $Ga^{3+}$ sites should be lower than $T_d$ and $O_h$. In fact, both kinds of $Ga^{3+}$ ions occupy 4*i* positions with the same site symmetry of $C_s$ in accordance with the $C2/m$ space group.[10] The single crystal NMR spectroscopy of β-$Ga_2O_3$ also verified the local mirror-plane symmetry of these two gallium sites.[48] Most importantly, the $C_s$ symmetry of $Ga^{3+}$ is also consistent with the site symmetry deduced by the PL spectra of $Eu^{3+}$ in this work. Because of the same symmetries for both crystallographic sites, it's difficult to determine the exact site of $Ga^{3+}$ that the $Eu^{3+}$ ions substitute for. Nevertheless, the ionic radii of the $Ga^{3+}$ ions are 0.047 and 0.062 nm for tetrahedral and octahedral coordination, respectively.[29,49] Taking into account the ionic radius of the $Eu^{3+}$ ions (0.095 nm), the distorted octahedral site should be more suitable to accommodate $Eu^{3+}$ ions. This is also in excellent agreement with foregoing spectral assignment because only a single lattice site of $Eu^{3+}$ was observed for the sample annealed at 1100 °C. The electron paramagnetic resonance (EPR) measurements of $Er^{3+}$-doped β-$Ga_2O_3$ single crystal also demonstrated that the incorporation of $Er^{3+}$ (ionic radius of 0.088 nm) occurred at a single crystallographic site.[27]

### 3.4 Crystal-field analysis

Generally, the CF interaction is relatively weak compared with electrostatic and spin–orbit coupling because the partially filled 4f shell is shielded by the filled 5s and 5p orbitals. The commonly used effective operator Hamiltonian is

$$H = H_{FI} + H_{CF}, \quad (1)$$

Where the free-ion (FI) Hamiltonian can be expressed as:

$$H_{FI} = E_{avg} + \sum_{k=2,4,6} F^k f_k + \zeta_f A_{SO} + \alpha L(L+1) + \beta G(R_2) + \gamma G(R_7) + \sum_{i=2,3,4,6,7,8} T^i t_i + \sum_{h=0,2,4} M^h m_h + \sum_{f=2,4,6} P^f p_f, \quad (2)$$

The physical meaning of these FI parameters has been described by Crosswhite and Carnall *et al.*[50,51] The single-particle CF Hamiltonian is expressed in Wybourne's notation,[52]

$$H_{CF} = \sum_{k,q} \mathrm{Re}B_q^k[C_q^k + (-1)^q C_{-q}^k] + i\mathrm{Im}B_q^k[C_q^k - (-1)^q C_{-q}^k] \quad (3)$$

For $Eu^{3+}$ ion at the $C_s$ site, $kq$ = 20, 22, 40, 42, 44, 60, 62, 64 and 66, with a total number of 15 CF parameters. A reflection plane is introduced to make the imaginary part of $B_2^2$ equal to zero, which reduces the total number of independent CF parameters from 15 to 14.

From the 10 K excitation and emission spectra of the sample annealed at 1100 °C, 71 CF levels of $Eu^{3+}$ in β-$Ga_2O_3$ have been identified. The CF levels of $Eu^{3+}$ were fitted at $C_s$ symmetry using the f-shell empirical programs from Reid.[53] The detailed fitting procedure is similar to that reported by Liu and Chen.[54] The FI parameters of $Eu^{3+}$ : $LaF_3$[51] and CF parameters of $Eu^{3+}$ : $Gd_2O_3$[54] were used as initial values for the fitting. The standard deviation of the final fit is 12.9 $cm^{-1}$, showing a good agreement between experimental and calculated values. Table 1 compares the experimental and fitted CF levels below 34 000 $cm^{-1}$. Table 2 lists the obtained FI and CF parameters. The derived FI parameters of $Eu^{3+}$ in β-$Ga_2O_3$ are close to those in $In_2O_3$,[6] but CF parameters differ appreciably in magnitude. Particularly, the $B_0^2$, Re $B_4^4$, Im $B_4^4$, $B_0^6$, Re $B_2^6$, Im $B_4^6$, Im $B_4^6$, Re $B_6^6$, and Im $B_6^6$ values have opposite signs, indicating a very different CF environment experienced by $Eu^{3+}$ in β-$Ga_2O_3$.

**Table 1** CF levels of $Eu^{3+}$ at the $C_s$ site of β-$Ga_2O_3$ at 10 K

| | Energy/cm$^{-1}$ | | | Energy/cm$^{-1}$ | | | Energy/cm$^{-1}$ | | | Energy/cm$^{-1}$ | | | Energy/cm$^{-1}$ | |
|---|---|---|---|---|---|---|---|---|---|---|---|---|---|---|
| SLJ | Exp. | Fit | SLJ | Exp. | Fit | SLJ | Exp. | Fit | SLJ | Exp. | Fit | SLJ | Exp. | Fit |
| $^7F_0$ | 0 | 4 | | 21 510 | 21 498 | | 26 483 | 26 471 | | — | 27 744 | | — | 31 290 |
| $^7F_1$ | 223 | 242 | | — | 21 526 | | — | 26 484 | | — | 27 751 | | 31 299 | 31 301 |
| | 401 | 402 | $^5D_3$ | 24 284 | 24 273 | | — | 26 495 | | — | 27 834 | | — | 31 313 |
| | 505 | 515 | | — | 24 293 | | 26 511 | 26 505 | | — | 27 838 | | — | 31 330 |
| $^7F_2$ | 899 | 887 | | 24 325 | 24 314 | | — | 26 521 | | — | 27 880 | | — | 31 349 |
| | 955 | 943 | | — | 24 335 | | — | 26 529 | | — | 27 883 | | — | 31 355 |
| | 1058 | 1061 | | — | 24 345 | | — | 26 546 | | — | 27 931 | | — | 31 368 |
| | 1115 | 1103 | | — | 24 356 | | — | 26 548 | | — | 27 964 | | 31 377 | 31 389 |
| | 1265 | 1264 | | — | 24 372 | | — | 26 563 | | — | 27 988 | | — | 31 391 |
| $^7F_3$ | 1836 | 1845 | $^5L_6$ | — | 24 758 | | — | 26 572 | | — | 28 038 | | — | 31 408 |
| | 1872 | 1858 | | — | 24 772 | | — | 26 573 | | — | 28 044 | | — | 31 421 |
| | 1902 | 1893 | | — | 24 833 | | — | 26 587 | | — | 28 080 | | — | 31 444 |
| | 1930 | 1933 | | 24 876 | 24 878 | | 26 617 | 26 612 | | — | 28 087 | | — | 31 469 |
| | 1986 | 1983 | | — | 24 921 | | — | 26 620 | | — | 28 101 | | — | 31 472 |
| | 2007 | 1990 | | 24 963 | 24 934 | | — | 26 668 | | — | 28 107 | | — | 31 473 |
| | 2086 | 2089 | | — | 24 978 | | — | 26 677 | | — | 28 120 | | — | 31 491 |
| $^7F_4$ | 2584 | 2599 | | 25 107 | 25 106 | | — | 26 713 | | — | 28 127 | | — | 31 494 |
| | — | 2792 | | 25 195 | 25 209 | | — | 26 721 | | — | 28 174 | | — | 31 504 |
| | 2812 | 2814 | | 25 253 | 25 257 | | — | 26 724 | | — | 28 186 | | — | 31 539 |
| | 2918 | 2913 | | — | 25 289 | | — | 26 741 | | — | 28 193 | | — | 31 567 |
| | — | 2952 | | 25 323 | 25 349 | | — | 26 744 | | — | 28 213 | | — | 31 570 |
| | 3038 | 3033 | | 25 400 | 25 370 | | — | 26 745 | | — | 28 317 | | — | 31 570 |
| | 3054 | 3057 | $^5G_{2,3}$ | — | 25 800 | | — | 26 776 | | — | 28 327 | | 31 596 | 31 586 |
| | — | 3130 | $^5G_{4,5}$ | — | 25 869 | | — | 26 788 | | — | 28 388 | | — | 31 621 |
| | — | 3204 | $^5G_6$ | — | 25 871 | | — | 26 799 | | — | 28 431 | | — | 31 649 |
| $^7F_5$ | — | 3741 | $^5L_7$ | — | 25 892 | | 26 817 | 26 805 | | — | 28 455 | | 31 676 | 31 679 |
| | — | 3745 | | 25 900 | 25 893 | $^5L_8$ | — | 26 933 | | — | 28 541 | | — | 31 690 |
| | — | 3881 | | — | 25 927 | | — | 26 949 | | — | 28 566 | | — | 31 696 |
| | — | 3957 | | 25 947 | 25 947 | | — | 26 972 | | — | 28 575 | | — | 31 722 |
| | — | 3991 | | 25 974 | 25 970 | | — | 26 974 | | — | 28 594 | | — | 31 731 |
| | — | 3994 | | 25 994 | 26 000 | | 27 020 | 27 033 | | — | 28 680 | | — | 31 761 |
| | — | 4024 | | — | 26 035 | | — | 27 054 | | — | 28 696 | | — | 31 792 |
| | — | 4106 | | — | 26 055 | | — | 27 089 | | — | 28 778 | | — | 31 809 |
| | — | 4147 | | — | 26 078 | | — | 27 094 | | — | 28 778 | | — | 31 834 |
| | — | 4203 | | 26 123 | 26 118 | | — | 27 166 | | — | 28 791 | | — | 31 834 |
| | — | 4271 | | — | 26 150 | | — | 27 188 | | — | 28 793 | $^3P_0$ | — | 32 366 |
| $^7F_6$ | — | 4846 | | — | 26 170 | | 27 218 | 27 199 | $^5H_{3,4}$ | — | 30 869 | $^5F_{2,3}$ | — | 32 854 |
| | — | 4858 | | 26 199 | 26 207 | | 27 278 | 27 269 | $^5H_{5,6}$ | — | 30 881 | | — | 32 879 |
| | — | 4933 | | — | 26 220 | | — | 27 290 | $^5H_7$ | — | 30 909 | | — | 32 895 |
| | — | 4941 | | — | 26 236 | | — | 27 316 | | — | 30 936 | | — | 32 948 |
| | — | 5037 | | 26 247 | 26 242 | | 27 322 | 27 332 | | — | 30 949 | | 32 960 | 32 954 |
| | — | 5060 | | — | 26 258 | | — | 27 337 | | — | 30 959 | | — | 32 967 |
| | — | 5221 | | 26 288 | 26 281 | | — | 27 349 | | 30 979 | 30 962 | | 33 014 | 33 015 |
| | — | 5235 | | — | 26 295 | $^5D_4$ | — | 27 472 | | — | 30 978 | | — | 33 031 |
| | — | 5286 | | — | 26 295 | $^5L_{9,10}$ | — | 27 499 | | — | 31 034 | | — | 33 050 |
| | — | 5316 | | — | 26 349 | | 27 533 | 27 528 | | — | 31 037 | | 33 102 | 33 104 |
| | — | 5327 | | — | 26 355 | | — | 27 548 | | 31 075 | 31 075 | | — | 33 162 |
| | — | 5462 | | — | 26 359 | | — | 27 564 | | — | 31 099 | | — | 33 194 |
| | — | 5463 | | — | 26 367 | | — | 27 574 | | — | 31 131 | $^5F_1$ | — | 33 324 |
| $^5D_0$ | 17 244 | 17 232 | | 26 385 | 26 397 | | 27 586 | 27 590 | | — | 31 162 | | — | 33 343 |
| $^5D_1$ | 18 975 | 18 959 | | — | 26 402 | | — | 27 609 | | — | 31 186 | | — | 33 356 |
| | 19 008 | 19 012 | | — | 26 422 | | 27 617 | 27 629 | | — | 31 205 | $^5F_4$ | — | 33 373 |
| | 19 033 | 19 053 | | — | 26 434 | | 27 647 | 27 643 | | — | 31 213 | | — | 33 397 |
| $^5D_2$ | 21 436 | 21 445 | | — | 26 436 | | — | 27 644 | | — | 31 229 | | — | 33 402 |
| | 21 450 | 21 464 | | 26 455 | 26 450 | | — | 27 696 | | — | 31 256 | | 33 445 | 33 462 |
| | 21 468 | 21 478 | | — | 26 468 | | 27 693 | 27 702 | | — | 31 285 | | | |

The scalar CF strength ($S$) that reflects the overall CF interaction in the crystal can be calculated using Chang's definition:[55]

$$S = \left\{ \frac{1}{3} \sum_{k=2,4,6} \frac{1}{2k+1} \left[ |B_0^k|^2 + 2 \sum_{q>0} (|\mathrm{Re}B_q^k|^2 + |\mathrm{Im}B_q^k|^2) \right] \right\}^{1/2} \quad (4)$$

the calculated value of $S$ is 546 cm$^{-1}$ for $Eu^{3+}$ : β-$Ga_2O_3$, which is smaller than those of the cubic phase $Eu^{3+}$ : $Y_2O_3$ (673 cm$^{-1}$),[56,57] $Eu^{3+}$ : $Lu_2O_3$ (718 cm$^{-1}$)[58,59] and $Eu^{3+}$ : $In_2O_3$ (790 cm$^{-1}$)[6] with $C_2$ symmetry but larger than that of $YAlO_3$ (464 cm$^{-1}$)[60] with $C_s$ symmetry. It was found that the CF strength of $Eu^{3+}$ decreases with increasing ionic radius of the host cations for the $M_2O_3$ series (M = In, Lu, Y and Gd).[6,61] However, the $Eu^{3+}$-doped β-$Ga_2O_3$ doesn't obey this law albeit the ionic radius of $Ga^{3+}$ is smaller than that of $In^{3+}$. The possible reason is that the crystal structure and site symmetry of $Eu^{3+}$ in β-$Ga_2O_3$ is different from those in $M_2O_3$ series. In fact,

 

**Table 2** FI and CF parameters of $Eu^{3+}$ at the $C_s$ site of β-$Ga_2O_3$ crystals (in $cm^{-1}$)[a]

| Parameters | Values | Parameters | Values |
|---|---|---|---|
| $E_{avg}$ | 63 304(15) | $P^2$ | 360 |
| $F^2$ | 81 280(57) | $B_0^2$ | 41(46) |
| $F^4$ | 61 647(93) | $B_2^2$ | −625(31) |
| $F^6$ | 40 535 | $B_0^4$ | −988(48) |
| $\xi$ | 1319(1) | Re $B_2^4$ | −397(89) |
| $\alpha$ | 20.16 | Im $B_2^4$ | −1243(42) |
| $\beta$ | −567 | Re $B_4^4$ | −165(71) |
| $\gamma$ | 1500 | Im $B_4^4$ | 223(48) |
| $T^2$ | 300 | $B_0^6$ | −1096(84) |
| $T^3$ | 40 | Re $B_2^6$ | −177(78) |
| $T^4$ | 60 | Im $B_2^6$ | −201(59) |
| $T^6$ | −300 | Re $B_4^6$ | 73(93) |
| $T^7$ | 370 | Im $B_4^6$ | 553(58) |
| $T^8$ | 320 | Re $B_6^6$ | 720(53) |
| $M^0$ | 2.1 | Im $B_6^6$ | 151(166) |
| rms[b] | 12.9 | | |

[a] Values in parentheses are errors in the indicated parameters which are freely varied in the fit. [b] The root-mean-square (rms) deviation between the experimental and calculated energies was used as a figure of merit to describe the quality of a fit, with $\text{rms} = \sqrt{\sum (E_{exp} - E_{calc})^2/(N-P)}$, where $N = 71$, the number of CF levels fit, and $P = 19$, the number of parameters freely varied.

not only ionic radius but also other factors including optical electronegativity, covalency, and structural distortion could influence the CF strength of $Eu^{3+}$. For instance, in contrary to the $M_2O_3$ series, the CF strength of $Eu^{3+}$ increases with increasing ionic radius of the host cations for LnOX series (Ln = Y, Gd, and La; X = Cl and Br).[60] The CF strengths of $Eu^{3+}$ in various crystals have been summarized by Chen and Liu.[60] A relatively large $S$ value can be found for $Eu^{3+}$-doped β-$Ga_2O_3$ because RE ions occupying a lower site symmetry normally have a larger CF strength.

### 3.5 Luminescence lifetime

PL decays of the $^5D_0$ multiplet were measured at 10–300 K for the sample annealed at 1100 °C (Fig. 7). All the curves exhibit nearly single exponential behavior and the fitted PL lifetime is 0.939 ms at 10 K. No rising time in the initial part of the decay curves can be observed within the detectable limit, in accordance with the efficient host-to $Eu^{3+}$ ET and multi-phonon relaxation from upper multiplets to $^5D_0$. The inset of Fig. 7 shows the dependence of temperature on the PL lifetime of $^5D_0$ at 3–300 K determined by single exponential fit. It can be found that the PL lifetime increases significantly as the temperature decreases from 150 to 30 K, but only changes insignificantly below 20 K. Therefore, it is reasonable to regard the observed $^5D_0$ lifetime at 10 K (0.939 ms) as the intrinsic radiative lifetime of $^5D_0$ for $Eu^{3+}$ in β-$Ga_2O_3$. Generally, the multiphonon nonradiative relaxation between $^5D_0$ and $^7F_6$ multiplets of $Eu^{3+}$ in β-$Ga_2O_3$ can be neglected because the energy gap between them (~12 000 $cm^{-1}$) is about 15 times the maximum phonon energy (~760 $cm^{-1}$) of β-$Ga_2O_3$.[62,63] Thus it is expected that the $^5D_0$ lifetime of $Eu^{3+}$ varies little with the temperature. Nevertheless the observed strong temperature-dependency of the $^5D_0$ lifetime

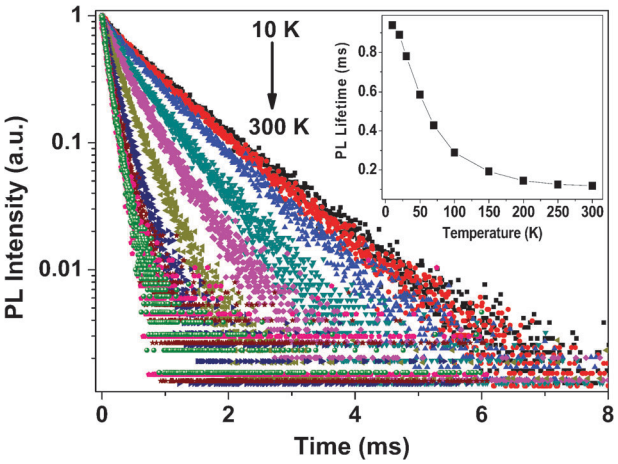


**Fig. 7** PL decays from $^5D_0$ measured at 10–300 K by monitoring the $^5D_0 \rightarrow {}^7F_2$ emission upon excitation at 266 nm for the sample annealed at 1100 °C. The inset shows the temperature dependence of the PL lifetime determined by single exponential fit.

(Fig. 7) indicates that a phonon-assisted nonradiative ET process could be the dominant nonradiative mechanism. Similar decay behaviors of $^5D_0$ were also observed in $Eu^{3+}$ : BaFCl,[64] $Cs_2NaEuCl_6$,[65] $EuAl_3B_4O_{12}$,[66] $EuMgB_5O_{10}$,[67] $Eu_2(MoO_4)_3$,[68] and $Eu_2O_3$ crystals.[69] The possible reasons for these unusual PL decay behaviors are due to: (1) ET from $^5D_0$ to the impurity ions or defects in those crystals; (2) ET between $Eu^{3+}$ ions occupying different crystallographic sites. Herein we infer that reason (1) may play the key role since no multiplet $Eu^{3+}$ sites were observed in our samples. The PL decay curves of the samples annealed at 650, 900 and 1000 °C at 10 K and RT were also measured, showing that they have nearly the same PL lifetimes as that of the sample annealed at 1100 °C. The PL lifetime of the sample annealed at lower temperature was expected to be shorter than that of the sample annealed at 1100 °C, in view of the existence of more defects such as oxygen vacancies in the sample annealed at lower temperature. However, the nearly same PL lifetime of different samples indicates that oxygen vacancies may not be the quenching centers of the $Eu^{3+}$ luminescence. The origin of the impurity ions or crystal defects remains unclear and needs further investigation.

The theory of diagonal phonon-assisted ET processes was systematically formulated by Holstein *et al.*, and the approximate temperature-dependent ET rates for different microscopic mechanisms were summarized.[64,70,71] The non-radiative ET rate ($W_{NR}$) of $Eu^{3+}$ in β-$Ga_2O_3$ at various temperatures was calculated based on the observed lifetimes ($\tau(T)$) using the formula $W_{NR} = \tau(T)^{-1} - \tau_0^{-1}$, where $\tau_0$ is the radiative lifetime (0.939 ms) of $Eu^{3+}$, and plotted in Fig. 8. The data can be well fitted according to the two-phonon assisted one-site resonant process using the following equation:[72]

$$W_{NR} = A + B\exp(-\Delta/k_B T), \quad (5)$$

where $\Delta$ is the energy splitting to a real state and $k_B$ is Boltzmann's constant. The fitted values are 1.39 × $10^5$ $s^{-1}$ for $A$, 1.31 × $10^7$ $s^{-1}$ for $B$, and 360 $cm^{-1}$ for $\Delta$. For this

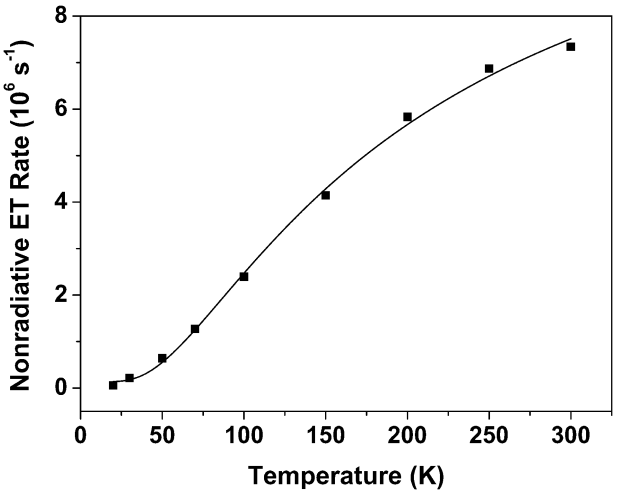


**Fig. 8** Nonradiative ET rate of $Eu^{3+}$ for the sample annealed at 1100 °C as a function of temperature. The scattering points are experimental data and the solid line denotes fitting results from eqn (5).

mechanism, a third electronic level near excited or ground state of donor ions is required. Obviously, for $Eu^{3+}$ ions, the third level could be near the ground state ($^7F_0$) since there is no such level in the proximity of $^5D_0$. The energy gap between $^7F_0$ and the second sub-level of $^7F_1$ is 401 $cm^{-1}$ in β-$Ga_2O_3$, which is close to 360 $cm^{-1}$ of $\Delta$. Thus this CF level of $^7F_1$ may act as the third level in the above ET process. The same ET mechanism was also observed in $Eu^{3+}$-to-$Nd^{3+}$ and $Eu^{3+}$-to-$Ni^{2+}$ ET processes in $EuMgB_5O_{10}$ crystals.[72]

## 4. Conclusions

The electronic structure and optical spectroscopy of $Eu^{3+}$-doped β-$Ga_2O_3$ NCs, synthesized by a simple combustion method, have been systematically investigated. The evolution of optical spectra with increasing the annealing temperature of NCs shows unambiguously that more $Eu^{3+}$ ions were incorporated into the crystal lattice with the growth of NCs. $Eu^{3+}$ ions were found to occupy only a single lattice site despite of two nonequivalent $Ga^{3+}$ sites in β-$Ga_2O_3$. Spectroscopic evidence revealed the local point-group symmetry of $C_s$ for $Eu^{3+}$ at this single site, and thus clarifies the previously controversial assignments. CF levels of $Eu^{3+}$ at the $C_s$ site with a total number of 71 have been identified and fitted in terms of 19 freely varied free-ions and CF parameters, which yielded a small standard deviation of 12.9 $cm^{-1}$. The $Eu^{3+}$ in β-$Ga_2O_3$ experiences a large CF strength of 546 $cm^{-1}$, which is consistent with the relatively low site symmetry ($C_s$) of $Eu^{3+}$. PL decays of the $^5D_0$ multiplet for $Eu^{3+}$ in the sample annealed at 1100 °C showed an unusual temperature-dependent behavior due probably to the ET from the excited $Eu^{3+}$ to impurity ions or crystal defects. The nonradiative ET mechanism of $Eu^{3+}$ involved may be dominated by the two-phonon assisted one-site resonant process, as evidenced by the dependence of temperature on the ET rate that obeys the function of $\exp(-\Delta/k_BT)$. The intrinsic radiative lifetime of $^5D_0$ of $Eu^{3+}$ in β-$Ga_2O_3$ was determined to be 0.939 ms. A comprehensive survey of electronic structure and optical properties of $Eu^{3+}$ in β-$Ga_2O_3$ nanophosphors is of crucial importance for their potential applications in the fields of optoelectronic devices, phosphors, biodetection or bio-imaging.

## Acknowledgements

This work is supported by the Hundred Talent Program of the Chinese Academy of Sciences (CAS), Knowledge Innovation Program of CAS for Key Topics (No. KJCX2-YW-358), the NSFC (Nos. 10974200 and 51002151), the 973 and 863 programs of MOST (Nos. 2007CB936703 and 2009AA03Z430), and the NSF of Fujian Province for Distinguished Young Scholars (Nos. 2009J06030, 2009J05138 and 2010J05126).

## Notes and references

1 Y. Hori, X. Biquard, E. Monroy, D. Jalabert, F. Enjalbert, L. S. Dang, M. Tanaka, O. Oda and B. Daudin, *Appl. Phys. Lett.*, 2004, **84**, 206.
2 Y. Q. Wang and A. J. Steckl, *Appl. Phys. Lett.*, 2003, **82**, 502.
3 R. Bilyy, A. Podhorodecki, M. Nyk, R. Stoika, A. Zaichenko, G. Zatryb, J. Misiewicz and W. Strek, *Physica E (Amsterdam)*, 2008, **40**, 2096.
4 H. Q. Wu, C. B. Poitras, M. Lipson, M. G. Spencer, J. Hunting and F. J. DiSalvo, *Appl. Phys. Lett.*, 2006, **88**, 011921.
5 O. Contreras, S. Srinivasan, F. A. Ponce, G. A. Hirata, F. Ramos and J. McKittrick, *Appl. Phys. Lett.*, 2002, **81**, 1993.
6 Q. B. Xiao, Y. S. Liu, L. Q. Liu, R. F. Li, W. Q. Luo and X. Y. Chen, *J. Phys. Chem. C*, 2010, **114**, 9314.
7 T. Miyata, T. Nakatani and T. Minami, *J. Lumin.*, 2000, **87–89**, 1183.
8 H. H. Tippins, *Phys. Rev.*, 1965, **140**, A316.
9 N. Ueda, H. Hosono, R. Waseda and H. Kawazoe, *Appl. Phys. Lett.*, 1997, **71**, 933.
10 S. Geller, *J. Chem. Phys.*, 1960, **33**, 676.
11 M. Ogita, K. Higo, Y. Nakanishi and Y. Hatanaka, *Appl. Surf. Sci.*, 2001, **175**, 721.
12 M. Ogita, N. Saika, Y. Nakanishi and Y. Hatanaka, *Appl. Surf. Sci.*, 1999, **142**, 188.
13 K. Shimizu, A. Satsuma and T. Hattori, *Appl. Catal., B*, 1998, **16**, 319.
14 E. Nogales, B. Mendez and J. Piqueras, *Nanotechnology*, 2008, **19**, 035713.
15 W. C. Herbert, H. B. Minnier and J. J. Brown, *J. Electrochem. Soc.*, 1969, **116**, 1019.
16 L. Binet and D. Gourier, *J. Phys. Chem. Solids*, 1998, **59**, 1241.
17 G. Blasse and A. Bril, *J. Phys. Chem. Solids*, 1970, **31**, 707.
18 X. T. Zhou, F. Heigl, J. Y. P. Ko, M. W. Murphy, J. G. Zhou, T. Regier, R. I. R. Blyth and T. K. Sham, *Phys. Rev. B: Condens. Matter Mater. Phys.*, 2007, **75**, 125303.
19 S. Cho, J. Lee, I. Y. Park and S. Kim, *Mater. Lett.*, 2002, **57**, 1004.
20 Y. P. Song, H. Z. Zhang, C. Lin, Y. W. Zhu, G. H. Li, F. H. Yang and D. P. Yu, *Phys. Rev. B: Condens. Matter Mater. Phys.*, 2004, **69**, 075304.
21 C. H. Liang, G. W. Meng, G. Z. Wang, Y. W. Wang, L. D. Zhang and S. Y. Zhang, *Appl. Phys. Lett.*, 2001, **78**, 3202.
22 J. Zhang, F. H. Jiang and L. D. Zhang, *Phys. Lett. A*, 2004, **322**, 363.
23 P. N. Favennec, H. Lharidon, M. Salvi, D. Moutonnet and Y. Leguillou, *Electron. Lett.*, 1989, **25**, 718.
24 E. Nogales, J. A. Garcia, B. Mendez and J. Piqueras, *Appl. Phys. Lett.*, 2007, **91**, 133108.
25 E. Nogales, J. A. Garcia, B. Mendez, J. Piqueras, K. Lorenz and E. Alves, *J. Phys. D: Appl. Phys.*, 2008, **41**, 065406.
26 T. Biljan, A. Gajovic and Z. Meic, *J. Lumin.*, 2008, **128**, 377.
27 J. Vincent, O. Guillot-Noel, L. Binet, P. Aschehoug, Y. Le Du, F. Beaudoux and P. Goldner, *J. Appl. Phys.*, 2008, **104**, 033519.
28 G. G. Li, C. Peng, C. X. Li, P. P. Yang, Z. Y. Hou, Y. Fan, Z. Y. Cheng and J. Lin, *Inorg. Chem.*, 2010, **49**, 1449.
29 W. Y. Shen, M. L. Pang, J. Lin and J. Fang, *J. Electrochem. Soc.*, 2005, **152**, H25.

 

30 M. L. Pang, W. Y. Shen and J. Lin, *J. Appl. Phys.*, 2005, **97**, 033511.
31 J. H. Hao, Z. D. Lou, I. Renaud and M. Cocivera, *Thin Solid Films*, 2004, **467**, 182.
32 P. Wellenius, A. Suresh and J. F. Muth, *Appl. Phys. Lett.*, 2008, **92**, 3.
33 P. Wellenius, E. R. Smith, S. M. LeBoeuf, H. O. Everitt and J. F. Muth, *J. Appl. Phys.*, 2010, **107**, 103111.
34 P. Gollakota, A. Dhawan, P. Wellenius, L. M. Lunardi, J. F. Muth, Y. N. Saripalli, H. Y. Peng and H. O. Everitt, *Appl. Phys. Lett.*, 2006, **88**, 221906.
35 E. Nogales, B. Mendez, J. Piqueras and J. A. Garcia, *Nanotechnology*, 2009, **20**, 115201.
36 G. C. Liu, X. C. Duan, H. B. Li and D. W. Liang, *Mater. Chem. Phys.*, 2008, **110**, 206.
37 H. B. Xie, L. M. Chen, Y. N. Liu and K. L. Huang, *Solid State Commun.*, 2007, **141**, 12.
38 J. S. Kim, H. E. Kim, H. L. Park and G. C. Kim, *Solid State Commun.*, 2004, **132**, 459.
39 J. S. Kim, H. E. Kim, A. K. Kwon, H. L. Park and G. C. Kim, *J. Lumin.*, 2007, **122**, 710.
40 V. Mahalingam, E. Bovero, P. Munusamy, F. C. J. M. van Veggel, R. Wang and A. J. Steckl, *J. Mater. Chem.*, 2009, **19**, 3889.
41 R. Roy, V. G. Hill and E. F. Osborn, *J. Am. Chem. Soc.*, 1952, **74**, 719.
42 T. Mizunashi and S. Fujihara, *Electrochem. Solid-State Lett.*, 2008, **11**, J43.
43 K. C. Sheng and G. M. Korenowski, *J. Phys. Chem.*, 1988, **92**, 50.
44 B. Bihari, H. Eilers and B. M. Tissue, *J. Lumin.*, 1997, **75**, 1.
45 N. Ueda, H. Hosono, R. Waseda and H. Kawazoe, *Appl. Phys. Lett.*, 1997, **70**, 3561.
46 T. Harwig and F. Kellendonk, *J. Solid State Chem.*, 1978, **24**, 255.
47 Q. Ju, Y. S. Liu, R. F. Li, L. Q. Liu, W. Q. Luo and X. Y. Chen, *J. Phys. Chem. C*, 2009, **113**, 2309.
48 T. Vosegaard, I. P. Byriel, L. Binet, D. Massiot and H. J. Jakobsen, *J. Am. Chem. Soc.*, 1998, **120**, 8184.
49 R. D. Shannon, *Acta Crystallogr., Sect. A: Cryst. Phys., Diffr., Theor. Gen. Crystallogr.*, 1976, **32**, 751.
50 H. M. Crosswhite and H. Crosswhite, *J. Opt. Soc. Am. B*, 1984, **1**, 246.
51 W. T. Carnall, G. L. Goodman, K. Rajnak and R. S. Rana, *J. Chem. Phys.*, 1989, **90**, 3443.
52 B. G. Wybourne, *Spectroscopic Properties of Rare Earths*, Interscience, New York, 1965.
53 M. F. Reid, f-shell empirical programs and examples, personal communication.
54 L. Q. Liu and X. Y. Chen, *Nanotechnology*, 2007, **18**, 255704.
55 N. C. Chang, J. B. Gruber, R. P. Leavitt and C. A. Morrison, *J. Chem. Phys.*, 1982, **76**, 3877.
56 R. P. Leavitt, J. B. Gruber, N. C. Chang and C. A. Morrison, *J. Chem. Phys.*, 1982, **76**, 4775.
57 M. J. Weber, *Phys. Rev.*, 1968, **171**, 283.
58 M. Karbowiak, E. Zych and J. Holsa, *J. Phys.: Condens. Matter*, 2003, **15**, 2169.
59 E. Zych, *J. Phys.: Condens. Matter*, 2002, **14**, 5637.
60 X. Y. Chen and G. K. Liu, *J. Solid State Chem.*, 2005, **178**, 419.
61 E. Antic-Fidancev, J. Holsa and M. Lastusaari, *J. Alloys Compd.*, 2002, **341**, 82.
62 D. Dohy, G. Lucazeau and A. Revcolevschi, *J. Solid State Chem.*, 1982, **45**, 180.
63 Y. H. Gao, Y. Bando, T. Sato, Y. F. Zhang and X. Q. Gao, *Appl. Phys. Lett.*, 2002, **81**, 2267.
64 X. Y. Chen, W. Zhao, R. E. Cook and G. K. Liu, *Phys. Rev. B*, 2004, **70**, 205122.
65 M. Bettinelli and C. D. Flint, *J. Phys.: Condens. Matter*, 1991, **3**, 7053.
66 F. Kellendonk and G. Blasse, *J. Chem. Phys.*, 1981, **75**, 561.
67 M. Buijs and G. Blasse, *Chem. Phys. Lett.*, 1985, **113**, 384.
68 M. Buijs, G. Blasse and L. H. Brixner, *Phys. Rev. B*, 1986, **34**, 8815.
69 M. Buijs, A. Meyerink and G. Blasse, *J. Lumin.*, 1987, **37**, 9.
70 T. Holstein, S. K. Lyo and R. Orbach, in *Laser Spectroscopy of Solids*, ed. W. M. Yen and P. M. Selzer, Springer, New York, 1981, p. 39.
71 W. M. Yen, in *Spectroscopy of Solids Containing Rare Earth Ions*, ed. K. A. A. and M. R. M., North-Holland, Amsterdam, 1987, p. 185.
72 M. Buijs and G. Blasse, *J. Lumin.*, 1986, **34**, 263.